21st European Conference on Fracture, ECF21, 20-24 June 2016, Catania, Italy

Interaction of strain rate and necking on the stress-strain response of uniaxial tension tests by Hopkinson bar

G. Mirone[a]*, D. Corallo[a], R. Barbagallo[a]

[a]University of Catania, Dept. of Industrial Engineering, Viale A. Doria 6, 95125, Catania, Italy

Abstract

The effect of the necking combined to that of the strain rate is analysed in dynamic split Hopkinson bar (SHTB) tests, by both experiments and finite elements. Experiments from the literature by Noble et al. are considered here together with other tests ran at the University of Catania. Two different characterization procedures are used for modeling the materials, leading to strain and strain rate-dependent flow stress according to the Johnson-Cook model for the Remco Iron by Noble et al., and to an MLR-based calibration for the FeN steel implemented by fortran subroutines, respectively.

After satisfactory validation of the finite elements results and of the dynamic hardening models via comparison to the experimental stress-strain, a detailed investigation on the way the necking perturbation of the stress interacts with the strain rate is carried out, expecially investigating how the ratio of the flow stress/true stress evolves with the strain and the strain rate.

Special modifications are introduced to the subroutine modeling the strain rate-promoted dynamic amplification of the stress; the related response from finite elements confirms the outcomes of previous papers, unveiling a new feature of the dynamic stress in SHTB tests and providing new information about the suitability and the accuracy of the modern procedures for the dynamic stress-strain characterization.

Keywords: Strain rate, Necking, True stress, Flow stress

* Corresponding author. Tel.: +39-95-7382418; fax: +39-95-330258.
  E-mail address: gmirone@dii.unict.it

1. Introduction

The procedure originally developed for the dynamic characterization via the SHTB, only based on strain gage measurements on the bars and delivering the engineering stress-strain curves, is nowadays outdated by the speed camera-assisted experimental procedures as in Noble et al. (1999), Verleysen et al.(2004), Sato et al.(2015), allowing to obtain the true stress-strain curves, also in the postnecking range.

In fact, the engineering stress-strain curves are much less accurate than true curves and, for the quasistatic stress-strain characterization, the former can only be used as a reference for iterative reverse engineering based on finite elements, where the flow curve of the material (equivalent stress vs. equivalent plastic strain) is iteratively changed until the engineering curve predicted by finite elements agrees with the experimental one.

Although the true curve is much more accurate than the engineering curve, it also diverges from the flow curve after necking and requires further refinements for becoming a reasonable approximation of the flow curve, like either the Bridgman correction or the finite elements based reverse engineering similar to that necessary with the engineering data.

A faster procedure was introduced for the quastistatc necking by Mirone (2004), transforming the postnecking true curve into an estimation of the flow curve by a simple corrective function *MLR*, independent of the material and capable of delivering an accuracy around 3%.

The necking under dynamic loading is an open issue attracting the interest of various researchers like Rusinek et al. (2005), Yang et al. (2005), Osovski et al. (2013), Besnard et al. (2012). The suitability of the above method for correcting also dynamic true curves was checked in Mirone (2013) with regard to the Remco iron tested by Noble et al (1999) and modeled through a Johnson-Cook formulation, but the flow stress/true stress ratio measured on the nodes of the evolving neck section resulted to significantly diverge from the *MLR* function; a perfect agreement was restored if only the flow stress for generating the above ratio was calculated by the Johnson-Cook formula, where the true strain and the engineering strain rate were introduced.

This outcome motivated further investigations, including experimental tests on a ductile steel here identified as FEN, together with various numerical simulations based on the experiments on both the Remco iron and the FEN steel, where the static part of the material model was left unaltered and only the dynamic amplification was changed according to different criteria.

The results obtained depict a new framework of the way the SHTB can (indeed cannot) be used for dynamic characterization of metals; the interaction of the strain and the strain rate after necking initiation is found to play a surprising role which can also prevent any possibility of a meaningful dynamic characterization, and also explains the apparent saturation of the dynamic amplification which is always included in the material models like the Johnson-Cook one.

2. SHTB experiments and camera-assisted dynamic characterization

The Remco iron from the work by Noble et al was modeled through the Johnson-Cook model according to eq. 1 .

$$\sigma_{Eq} = \left(175 + 380 \cdot \varepsilon^{0.32}\right) \cdot \left(1 + 0.06 \cdot \ln \dot{\varepsilon}\right)\left(1 - T^{*0.55}\right) \tag{1}$$

The dynamic amplification of the flow stress is the strain rate-dependent term in the second bracket of eq. (1).
The above parameters, used for implicit f.e. analyses in Mirone 2013, briefly recalled below, allowed to correctly reproduce the experimental area reduction measured by fast image acquisition, as in the right side plot of Figure 1, also reporting, on the left side, the trend of the dynamic amplification included in eq. 1.
Once the Johnson-Cook calibrated model by Noble et al. was validated, further analyses were ran with the same material model, simulating two different incident waves and two specimen lengths, (four different strain rates), in order to investigate the correspondidng variations of the stress-strain response and to check whether or not the ratio $\sigma_{Eq}/\sigma_{True}$ evolved according to the *MLR* function. Figure 2 shows the incident waves imposed to the modeled input bar, and the corresponding evolutions of the true strain rate vs. true strain, measured on the deforming nodes of the neck section.
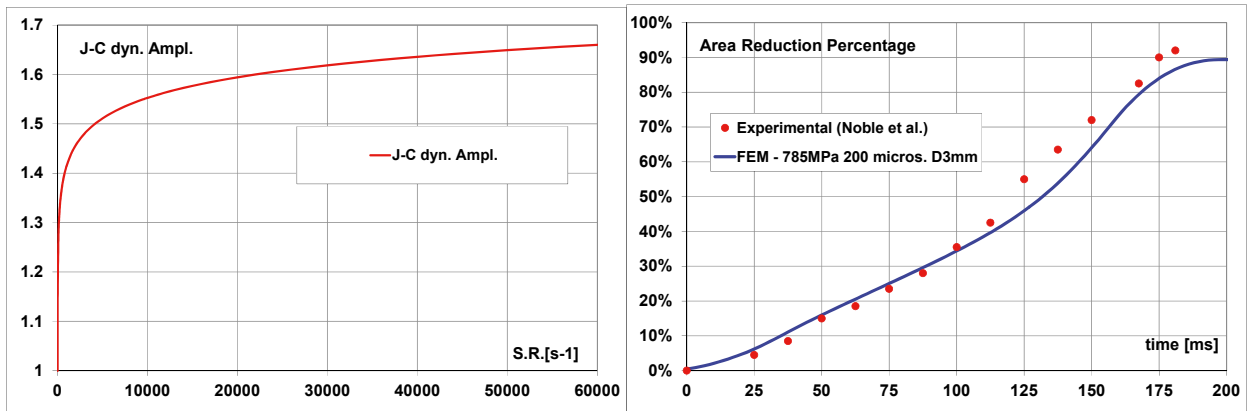
Figure 1: experimental valiudation of the material parameters for the Remco Iron (Mirone 2013)
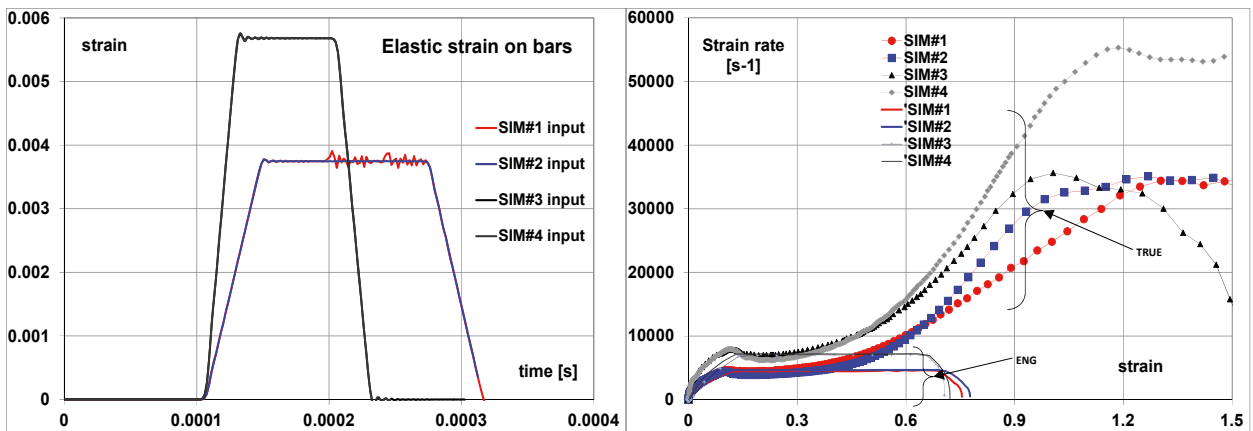

Figure 2: Incident waves and true strain rate s simulated on the Remco Iron
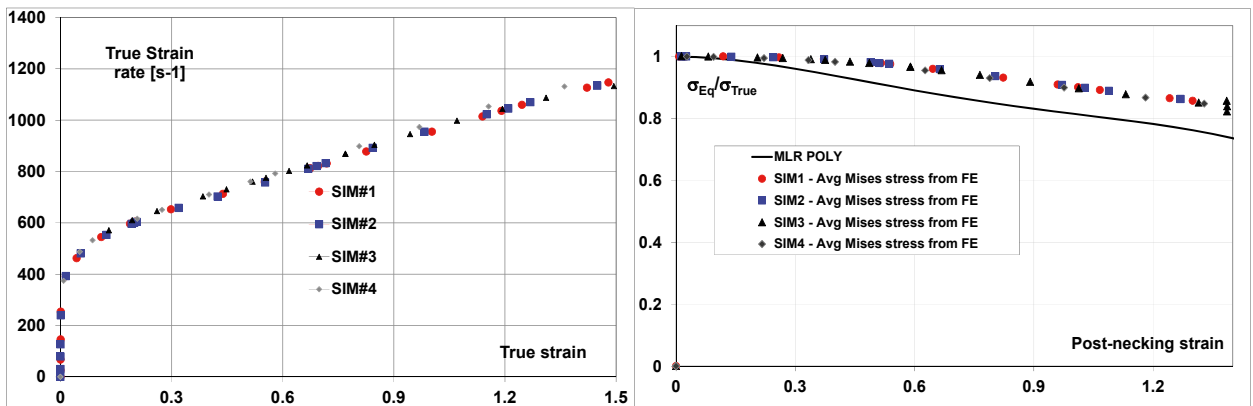

Figure 3: Mises stress/True stress ratio against MLR function for the Remco Iron

It is worth noting that, after necking initiation, the true strain rate vs. true strain curves largely diverge from the corresponding curves expressing the engineering strain rate vs. eng. strain, as properly depicted in Figure 2. After such departure, the true strain rate is increased up to 6-8 times more than the engineering one.

The stress-strain data predicted by the above four analyses and the corresponding ratio between true stress and Mises stress are reported in Figure 3, showing that the true curves are almost independent of the strain rate imposed to the specimens, and the postnecking ratio flow stress/true stress diverges significantly from the *MLR* function.

In the same paper was found that, if the equivalent stress for the above ratio was calculated by introducing the true strain and the engineering strain rate into the Johnson-Cook function, then a very good agreement was restored between the ratio and the MLR function, as visible in Figure 4.
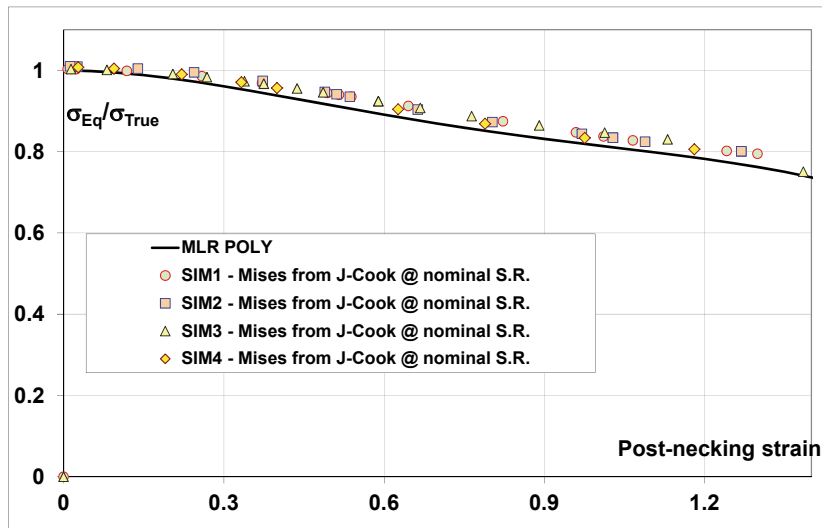

Figure 4: Flow stress /True stress ratio based on the true strain and the engineering strain rate

The only difference between the two evaluations of the flow stress lies in the strain rate adopted; when the "true" strain rate measured locally is used then the flow stress / true stress ratio differs from the MLR, instead, when the nominal "engineering" strain rate is used for calculating the flow stress, the MLR perfectly applies. The reasons of this outcome was only partially explained in Mirone (2013), so further investigations leading to the present paper were conducted.

A similar experimental – numerical procedure is carried out for a mild steel FE360 identified as FEN, and discussed in Mirone et al. (in review for J. Imp. Eng.), briefly recalled ahead. Specimens according to Figure 5 are tested, in a quasistatic motor driven testing machine and in a direct tension SHTB with 4.5 and 3 meters long input and output bars, respectively, all with 16 mm diameter and made of Al7075 alloy. Specimens with three gage lengths are adopted so L0 is 6, 9 and 12 mm. The incident wave is generated according to the Albertini and Staab-Gilat architecture, by preloading the first segment of the input bar 1.5 m long, and by abruptly releasing the preload through the fracture of a fragile element. The shrinking specimen shape is acquired by fast camera acquisition as in Figure 5 and by successive image analysis.
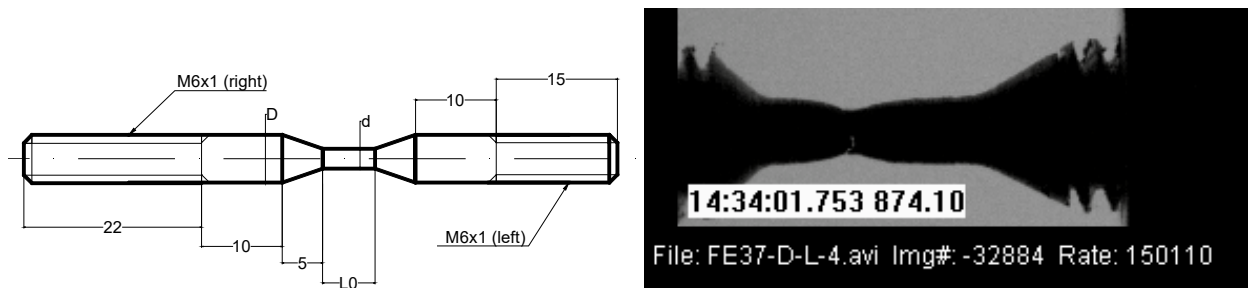

Figure 5: FEN specimens shape

Different incident waves are generated along the input bar of the SHTB, with a nominal duration of about 750 microseconds, a rise time of about 130 microseconds and different amplitudes, corresponding to input bar preloads from 15 to 75 kN; The quasistatic true curves and the most representative of the dynamic ones are reported in Figure 6 for the FEN steel, together with the corresponding true strain rates; the paper Mirone et al. (in review for Int. J. of Plast.) will be avalable for further details.
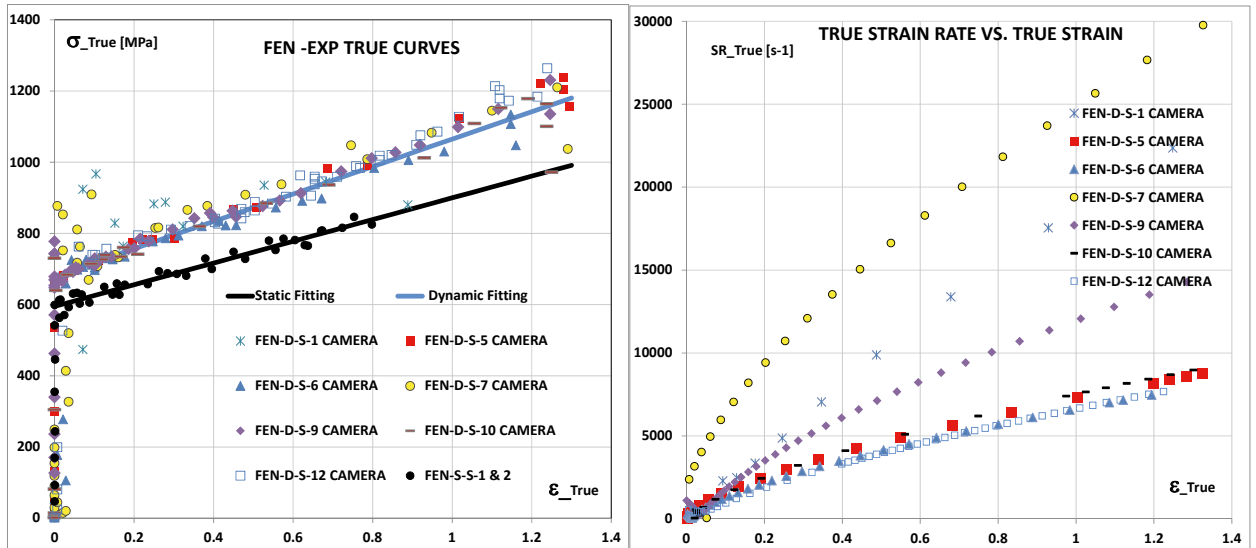

Figure 6: Experimental true curves and strain rates the FEN steel

Despite the true strain rates varies in a fivefold range, the experimental response is almost independent of the strain rate and all the true curves are almost overlapped within the limit of a visible but reasonable experimental scattering, similarly to what was found for the Remco iron. This independence of the strain rate, coupled to the significant difference visible between the static and the dynamic dynamic true curves, usually is interpreted as the result of a strong saturation of the strain rate effect at very low strain rates, placed somewhere between the quasistatic one and the lowest strain rate tested.

The doubts raised by such experimentally-based consideration pushed toward checking whether or not the same results were obtained by material characterization and successive finite elements simulations of the tests.

The dynamic characterization of the FEN steel is performed by assuming a more general function than the Johnson-Cook law:

$$\sigma_{Eq}\left(\varepsilon_{Eq}, \dot{\varepsilon}_{Eq}\right) = \sigma_{Eq\_S}\left(\varepsilon_{Eq}\right) \cdot R\left(\dot{\varepsilon}_{Eq}\right) \tag{2}$$

where the dynamic hardening is still obtained by two uncoupled multiplicative terms (the temperature effect is neglected here), the first expressing the quasistatic flow stress (depending on the strain alone) and the second expressing its dynamic amplification (depending on the strain rate alone), respectively.

The quasistatic flow stress is easily obtained according to Mirone (2004) by the *MLR* correction of the quasistatic true curve in the postnecking strain range:

$$\sigma_{Eq\_S}\left(\varepsilon_{Eq}\right) = \sigma_{True\_S}\left(\varepsilon_{Eq}\right) \cdot MLR\left(\varepsilon_{PostNeck}\right) \tag{3}$$

but, according to the present knowledge, the dynamic amplification R cannot be derived in any exact way because there is not any possibility of whether measuring or calculating the exact postnecking flow stress from any dynamic experiment.

Then an approximate hypothesis is adopted here, supposing that the dynamic amplification R of the flow stress is similar to the dynamic amplification *RTrue* of the true stress, which instead is perfectly measurable:

$$R\left(\dot{\varepsilon}_{Eq}\right) = \frac{\sigma_{Eq}\left(\varepsilon_{True}, \dot{\varepsilon}_{True}\right)}{\sigma_{Eq\_S}\left(\varepsilon_{True}\right)} \approx \frac{\sigma_{True}\left(\varepsilon_{True}, \dot{\varepsilon}_{True}\right)}{\sigma_{True\_St}\left(\varepsilon_{True}\right)} = R_{True}\left(\dot{\varepsilon}_{Eq}\right) \tag{4}$$

equation (4) is fully valid before necking because the true stress and the flow stress are identical each other, but after necking initiation it only represents an approximate hypothesis. However, the linear functions bestfitting the quasistatic and the dynamic true curves are divided each other at each given strain and strain rate of the loading histories experimentally imposed, delivering the dynamic amplification plotted on the left side of Figure 7.

The function *R* at very low strain rates must start from one because, by definition, no dynamic amplification occurs at quasistatic strain rates; then a steep linear ramp at strain rates from 0 to 100 s-1 is added, although this very early stage of dynamic tests is not catched by experiments because a very small time resolution would be necessary for sampling true curves points in the elastic range or at very early plastic stages, when the dynamic amplification is still starting to depart from one. If also viscoelastic effects occur, then also the first yield can be affected and smaller or no chamfer ramp at all can be necessary.

The *R* function obtained monotonically increases with no saturation all over the range of experimental strain rates; so, according to the same considerations made before with the Remco iron by Noble et al., it is difficult to explain why the very different strain rates imposed to the FEN, together with the non-saturating amplification found from the static and dynamic true curves, produced a single dynamic true curve although the imposed dynamic strain rates were very different each other.

The general uncoupled dynamic material model of eq. 2 is then implemented in finite element analyses (fea) simulating the experiments with the FEN steel, including the quasistatic true curve of Figure 6 and the dynamic amplification in Figure 7. Expectations were that no saturation in the dynamic hardening would have brought fea-estimated true curves quite different from the experimental ones and strongly strain rate-dependent.
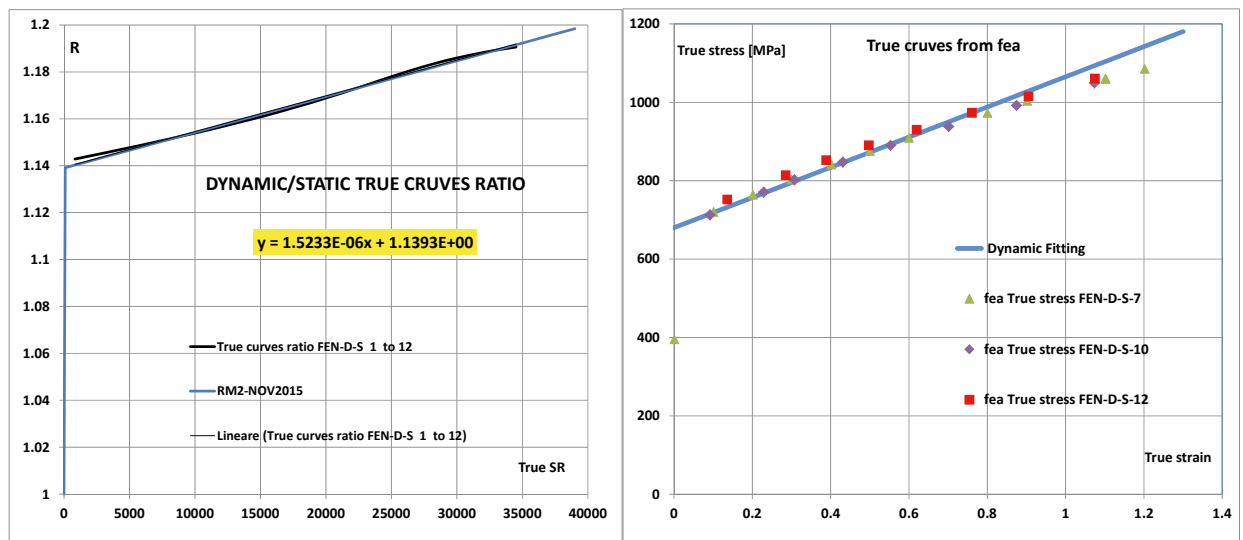

Figure 7: Approximate dynamic amplification for the FEN steel

The axial stress and the equivalent plastic strain from finite elements are then averaged over the neck cross section at selected analyses steps for the three most representative fea analyses (maximum and minimum strain rates, all three gage lengths).

The fea-predicted true curves generated in this way (dotted curves on the right side of Figure 7) are compeared to the bestfit of the experimental dynamic true curves.

It is rather surprisingly to see that the non-saturating dynamic amplification, together with the very different strain rates imposed, produced again a single dynamic true curve, as also the experiments did. The consideration that the fea true curve is well coincident to the experiments, and that this finding validates the material model is almost secondary, as the main point raised by these observations and requiring explanations is the apparent strain rate independence of the true curves despite the remarkable strain rate dependence implemented. By the way, for these

simulations the MLR postnecking correction applied very well, as shown in Figure 8

In the next sections, an explanation is found for the above response of both experiments and plasticity equations integrated by fea; an effect of the necking in combination with the strain rate and the strain rate history in time is highlighted, posing important limitations to the dynamic stress-strain characterization; the results of various fea analyses are commented, where variations are introduced to the dynamic amplification and/or to a specific feature of the incident waves, for confirming the above effect and the implications it has on the experimental characterization at dynamic strain rates.
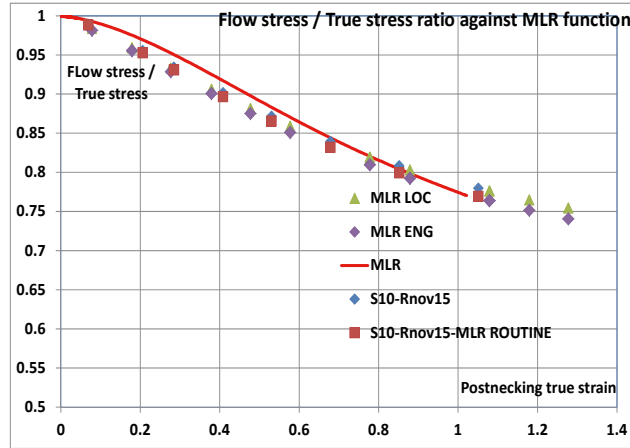

Figure 8: Flow stress / true stress ratio for the FEN steel

3. Interaction of necking and strain rate history

The key element complying with all the above responses is that the necking initiation is found to freeze the dynamic amplification of the true curves, while leaving undisturbed the amplification of the flow stress.

This hypothesis explains at the same time why the dynamic true curves at very different strain rates are frequently overlapping each other although being significantly different from the quasistatic ones, and why the ratio of dynamic flow stress to dynamic true stress sometimes does not follow the MLR function, although the adoption of the engineering strain rate for calculating a virtual flow stress only amplified by a "necking-free" strain rate, recovers the good agreement of the above ratio with the MLR function.

For checking this hypothesis, compatible with the experimental data and with the fea results already discussed, a further series of three specially "varied" fea runs is performed, aimed at simulating tests similar to those of the previous section, where special modifications are introduced for allowing to infer or to exclude causality between the different issues still open. The following observations are preliminary to all the "varied" analyses.

While the ratio $\sigma_{Eq}/\sigma_{True}$ for the static loading always follows the MLR polynomial, it seems that for the dynamic loading it can either evolve according (FEN steel) or in disagreement (Remco iron by Noble) with the MLR.

Then a quantity *DN* is defined here, function of the strain and/or of the strain rate, which quantifies the disagreement between the above ratio and the *MLR* polynomial:

$$\frac{\sigma_{Eq}\left(\varepsilon_{True},\dot{\varepsilon}_{True}\right)}{\sigma_{True}\left(\varepsilon_{True},\dot{\varepsilon}_{True}\right)} = MLR\left(\varepsilon_{True}\right)\cdot DN\left(\varepsilon_{True},\dot{\varepsilon}_{True}\right) \tag{5}$$

If *DN* = 1 then the *MLR* perfectly applies as for the FEN steel, otherwise a certain disagreement occurs between the ratio $\sigma_{Eq}/\sigma_{True}$ and the *MLR* , as for the Remco iron by Noble et al.

Then the approximate equation (4) can be rewritten in exact form as in eq. (6)

$$R\left(\dot{\varepsilon}_{Eq}\right) = \frac{\sigma_{Eq}\left(\varepsilon_{True},\dot{\varepsilon}_{True}\right)}{\sigma_{Eq\_S}\left(\varepsilon_{True}\right)} = R_{True}\left(\dot{\varepsilon}_{Eq}\right)\cdot DN\left(\varepsilon_{True},\dot{\varepsilon}_{True}\right) \tag{6}$$

The first special analysis is performed on a "depurated" Remco Iron where DN, intrinsically included in the parameters of the Johnson-Cook dynamic amplification, is calculated as the ratio of the curves in the left-side plot of Figure 3 and is eliminated from the hardening of the Remco iron by dividing the Johnson-Cook function by DN. The resulting "depurated" Remco is then modeled as follows:

$$\sigma_{Eq} = \left(175 + 380 \cdot \varepsilon_{True}^{0.32}\right) \cdot \frac{\left(1 + 0.06 \cdot \ln \dot{\varepsilon}\right)}{DN\left(\varepsilon_{True}, \dot{\varepsilon}_{True}\right)} \left(1 - T^{*0.55}\right) \tag{7}$$

Where the function DN is plotted on the left in Figure 9 together with the dynamic amplification of the original REMCO and of the "depurated" REMCO. The departure point of the two amplifications occurs at the strain rate of about 3500 s^{-1} occurring when the necking initiates due to the given incident wave; a different incident wave causes a different strain rate at incipient necking, then the DN function also depends on the loading history and is not a purely material-dependent function.
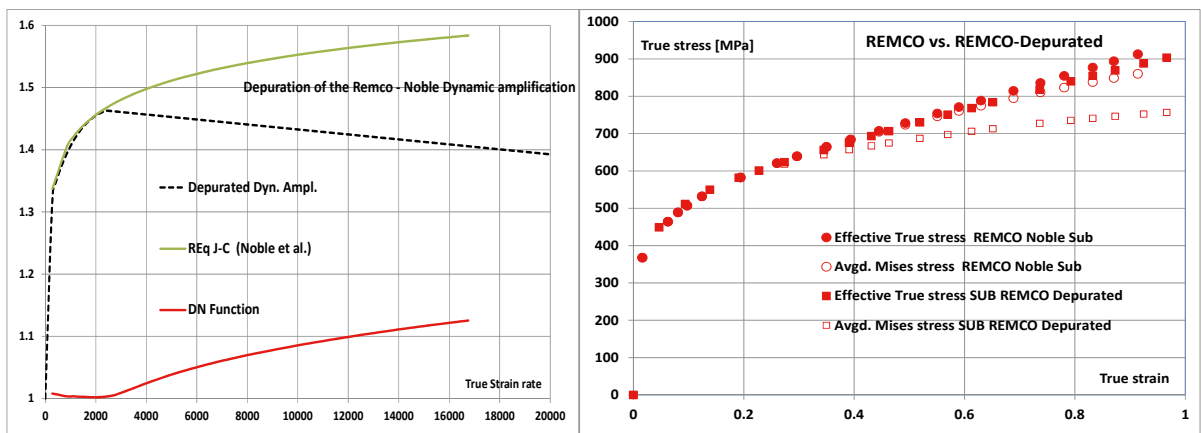

Figure 9: DN function and REMCO Dynamic amplification with / without depuration

The depurated amplification exhibits a descending trend after necking initiation, which corresponds to a strain rate-promoted material softening; then such depurated dynamic amplification mainly expresses a mathematical abstract concept and does not necessarily reflect the response of common structural metals.

The stress-strain response predicted by fea with the depurated REMCO material is compared in the right side of Figure 9 to the similar response of the original REMCO hardening by Noble et al.

It is evident that the true curves are almost insensitive to the changes of the dynamic amplification while, on the contrary, the flow curves are directly affected by it, as obviously required by equations (1) and (7).

The ratio $\sigma_{Eq}/\sigma_{True}$ now complies very well with the MLR polynomial as visible in Figure 10 where it is plotted together with the results from the original REMCO hardening by Noble et al. This gives one more confirmation that the modification in eq (7) was correctly performed and that, according to the equations of the time-dependent associate plasticity, such variation of the dynamic amplification in the postnecking range significantly affected only the flow stress while leaving almost unaltered the true stress.

The second fea analysis simulating modifications with respect to the experiments, is aimed at confirming that the function DN also depends on the strain history, which is generated through the incident wave on the input bar of the SHTB.

According to the hypothesis made, the dynamic amplification equally affects the true curve and the flow curve only before necking (and this is trivial as the true stress and the flow stress of smooth tensile specimens are coincident each other until necking); then, the dynamic amplification of the flow stress continues its evolution according to the strain rate history, while the amplification of the true stress remains frozen at the amplification level occurring at

the necking. Then this second simulation is made on the same REMCO-Depurated material model, but now a much less intense incident wave (V-Slow in Figure 11) is generated on the input bar, for inducing a lower strain rate on the specimen at incipient necking.
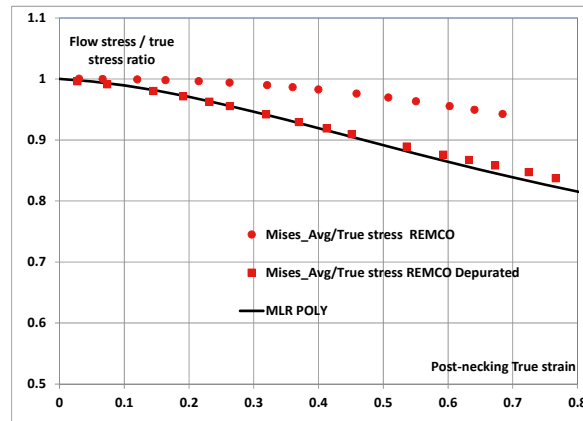

Figure 10: MLR ratio for the standard and the "depurated" REMCO iron

The right-side plot in Figure 11 reports the true strain rate vs. true strain for the two last analyses discussed, showing that the wave *V-Slow* generates a strain rate below 1000 s^{-1} at necking initiation (necking strain of REMCO is always close to 0.2), while the wave *V4* of the previous analyses generates a strain rate close to 3500 s^{-1} at incipient necking.
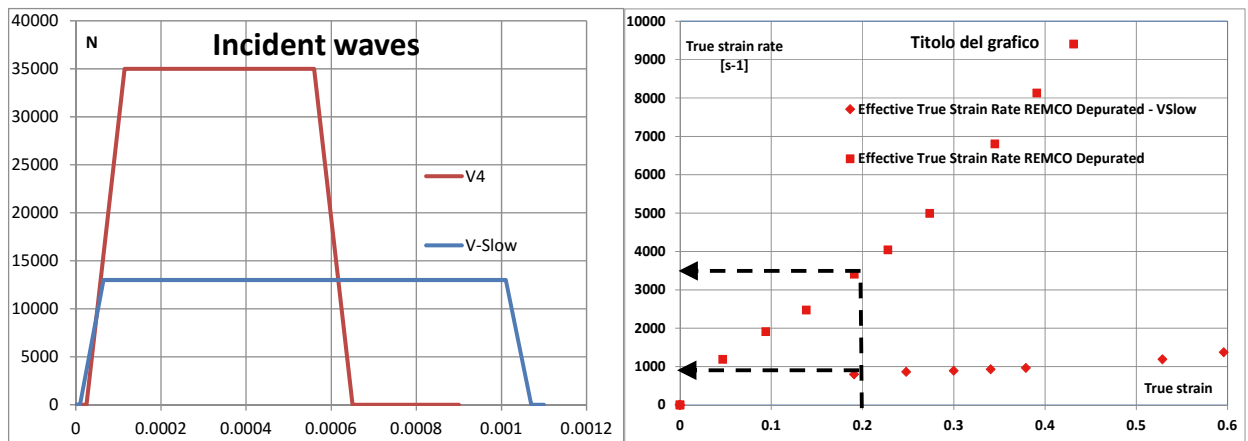

Figure 11: Incident waves and corresponding histories of true strain rate vs. true strain

The above changes in the incident wave and in the history of strain rate vs. strain cause the stress-strain curves and the ratio $\sigma_{Eq}/\sigma_{True}$ to significantly change as well as in Figure 12, despite the REMCO-Depurated material hardening law of eq (7) is left unaltered.

The point is that the low-amplitude wave *V-Slow* makes the strain rate at incipient necking quite smaller than that of the wave V4, so that the freezing effect of necking on the dynamic amplification of the true curve is anticipated.

The third analysis is somehow complementary to the first one; in fact, now the material model of the FEN steel is modified by introducing a function DN with arbitrary values, capable of artificially spoiling the dynamic amplification at strain rates beyond those at which necking initiates for the current loading wave *V4*.

In this way it is expected that the true curve is not affected by the modification and remains close to the experiments, while the flow curve is affected by it; then the ratio $\sigma_{Eq}/\sigma_{True}$, originally well compliant to the *MLR* function, should

diverge due to the spoiling effect of the arbitrary *DN* function.

The original dynamic amplification of the FEN steel is plotted in Figure 13 together with the arbitrary DN spoiling function and with the resulting spoiled dynamic amplification.
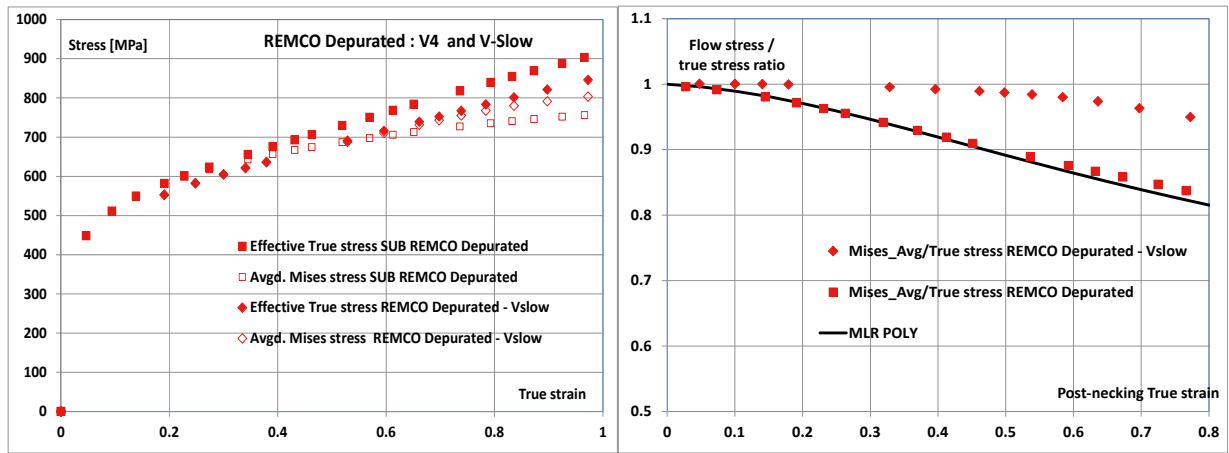

Figure 12: Effect of the incident wave on the dynamic amplification
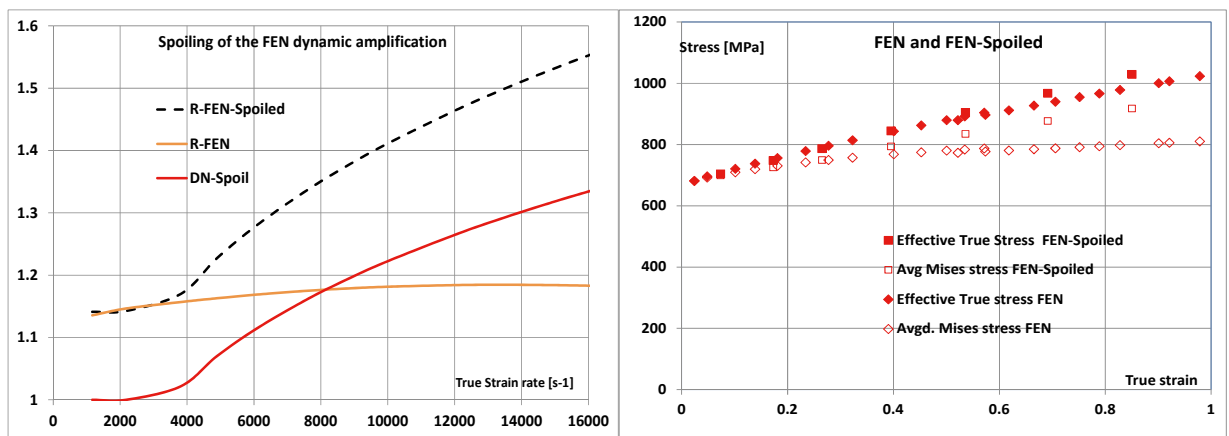

Figure 13: Dynamic amplification and stress-strain curves of the FEN steel, with and without spoiling function

Figure 13 also confirms that the spoiling introduced in the dynamic amplification function, only taking place after necking initiation from the wave V4, largely affects the flow stress while leaving unaltered the true stress. As a consequence the ratio $\sigma_{Eq}/\sigma_{True}$, perfectly following the *MLR* polynomial for the original FEN hardening function, now largely departs from it after the spoiling function is introduced.

All the above analyses confirm that, according to the equations of plasticity integrated by finite elements, the dynamic amplification of the true stress is stopped by the occurrence of the necking, while that of the equivalent stress is not affected by the necking and then freely evolves according to the local strain rate, which usually increases monotonically well beyond the nominal engineering strain rate (6 to 8 times more for the REMCO iron) because of the whole necking.

This means that many different dynamically amplified flow curves, following a common trend before necking but arbitrarily departing after necking initiation, can produce the same true curve. In turn, this implies that the one-to-one correspondence between true stress and flow stress, typical of the quasistatic loading histories, does not apply anymore to the case of dynamically loaded tensile specimens.
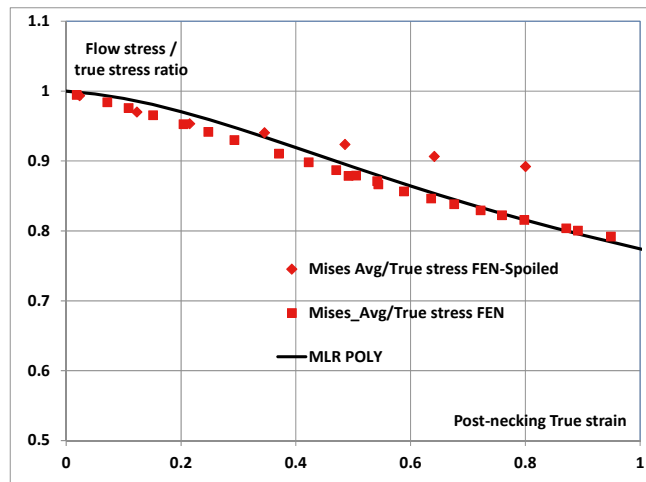
Figure 14: Flow stress/True stress ratio for the FEN steel with and without spoiling function

In other words, it seems that the dynamic stress-strain characterization in the postnecking range is virtually impossible because, all over such localization regime, the only measurable entity is the true curve and it may correspond to infinite different flow curves, with no apparent criteria available for selecting one instead of another.
A worth noting consideration is that the dynamic amplification R with $DN=0$, equivalent to the condition that $R=R_{True}$ and being the only one for which the *MLR* perfectly applies, also represents the lower boundary of the set of flow curves capable of generating the same true curve for a given loading history; it is likely that this finding implies further connections and relationships still to be found but, of course, at the moment this is not a valid reason for considering such a criteria sufficient for selecting the curve with $DN=0$ as the right flow curve among the above set.
It is also important to mention that, according to the finding discussed here, the dynamic stress-strain characterization is much more difficult for those materials exhibiting low necking strains, because they may require very sharp waves with very short rise times for achieving reasonable strain rates within necking initiation.

4. Conclusions

Dynamics SHTB experiments by Noble et al. and by the authors of the present paper have been used for characterizing the dynamic hardening of a Remco iron and of a FE 370 steel. Two dynamic hardening functions according to the Johnson-Cook model and according to a similar but more general formulation are adopted for the Remco and for the FEN steel, respectively.
The finite elements analyses based on both formulations returned local postnecking data in good agreement with experiments, apparently providing a validation of the hardening functions adopted.
Other fea have been ran, including modifications of the dynamic hardening and of the load history imposed through the incident waves; such analyses shown that the one-to-one relationship between true curves and flow curves typical of the quasistatic plasticity, no longer applies, because the necking stops the strain-rate-promoted amplification of the true curve, while leaving undisturbed the similar amplification the strain rate operates on the flow stress.
The freezeing effect caused by the necking on the true curves is fully compatible with the discussed experiments in a one-way sense, because such tests, although generating very different strain rate histories which significantly departed each other only after the necking, exhibited perfectly overlapping true curves. Further experiments should be identified and carried out for closing the loop of a two-way cause-effect relationship between the above hypothetical phenomena and experimental evidence, by proving that the same materials, when subjected to the proper strain histories, are capable of exhibiting different experimental true curves.

The above effect of necking seems to be also naturally included in the equations of the time-dependent implicit plasitity which are integrated by fea, as the different analyses above proved in various different situations.

The phenomena identified implies that, until no further findings show up allowing to discern the right flow curve among a set of infinite ones, the dynamic stress-strain characterization can be carried out only before necking initiation, and for materials with very low necking strain the it is virtually impossible at all.

The only difference marking a single flow curve among the set of those related to the same true curve, is that the lowest one of the set corresponds at the same time to the three condition that *DN=0* , that *R=RTrue* and that the ratio $\sigma_{Eq}/\sigma_{True}$ accurately follows the *MLR* polynomial, which for the static stress-strain characterization was proved to apply with a good engineering accuracy. This is not enough for identifying such a curve as the one really acting at the local scale on single material points, but certainly highlights it as a subject for further investigations.

References

Besnard, G., Hild, F., Lagrange, J. M., Martinuzzi, P., Roux, S., 2012. Analysis of necking in high speed experiments by stereocorrelation, International Journal of Impact Engineering. 49, 1353–1367

Mirone, G., 2004. A new model for the elastoplastic characterization and the stress–strain determination on the necking section of a tensile specimen. Int J Solids Struct 5(41), 3545–64.

Mirone, G. 2013. The dynamic effect of necking in Hopkinson bar tension tests, Mech. Mater. 58, 84-96.

Nilsson, K., 2004. Effects of elastic unloading on multiple necking in tensile bars, International Journal of Impact Engineering. 30, 1353–1367

Noble, J.P., Goldthorpe, B.D., Church, P. Harding, J., 1999. The use of the Hopkinson bar to validate constitutive relations at high rates of strain. Journal of the Mechanics and Physics of Solids 47, 1187–1206.

Osovski, S., D. Rittel, J.A., Rodríguez-Martínez, R., Zaera, 2013. Dynamic tensile necking, Influence of specimen geometry and boundary conditions, Mechanics of Materials 62, 1–13.

Rodríguez, J.A., Martínez, D., Rittel, R., Zaera, S., Osovski, 2013. Finite element analysis of AISI 304 steel sheets subjected to dynamic tension, The effects of martensitic transformation and plastic strain development on flow localization, 54, 206-216.

Rusinek, A., R., Zaera, J.R., Klepaczko, R., Cheriguene, 2005. Analysis of inertia and scale effects on dynamic neck formation during tension of sheet steel , Acta Materialia 53, 5387–5400.

Sato, K., Yu, Q., Hiramoto, J., Urabe, T., Yoshitake, A., 2015. A method to investigate strain rate effects on necking and fracture behaviors of advanced high-strength steels using digital imaging strain analysis, International Journal of Impact Engineering 75, 11-26.

Verleysen, P., Degrieck, 2004, Experimental investigation of the deformation of Hopkinson bar specimens J., International Journal of Impact Engineering 30, 239–253.

Yang, L.M., Shim, V.P.W., 2005. An analysis of stress uniformity in split Hopkinson bar test specimens, International Journal of Impact Engineering 31, 129–150.